Deep-Sea Research II ▮ (▮▮▮▮) ▮▮▮–▮▮▮

Contents lists available at ScienceDirect

Deep-Sea Research II

journal homepage: www.elsevier.com/locate/dsr2

Assimilation of HF radar-derived radials and total currents in the Monterey Bay area

Igor Shulman [a,*], Jeffrey D. Paduan [b]

[a] Naval Research Laboratory, Code 7331, Building 1009, Room A144, Stennis Space Center, MS 39529-5004, USA
[b] Naval Postgraduate School, Monterey, USA

ARTICLE INFO

Article history:
Accepted 16 August 2008

Keywords:
Ocean data assimilation and reanalysis
Coastal processes
Currents
Ocean observing systems
Upwelling

ABSTRACT

Impact of HF radar surface-current assimilation on ocean circulation model predictions in the Monterey Bay area is studied and evaluated during the time frame of the Autonomous Ocean Sampling Network (AOSN-II) experiment (August–September 2003). In the first instance, a previously described method for assimilation of surface current data is applied to 33-h low-pass-filtered data and a non-tidal version of the circulation model. It is demonstrated that assimilation of surface velocity data significantly improves the surface and subsurface correlation of model currents with moored current observations. These results from the AOSN-II period illustrate that surface-current assimilation is beneficial even in cases for which very high-resolution (3 km) atmospheric forcing is utilized. The assimilation approach is also tested with hourly, unfiltered, CODAR-type HF radar-derived surface currents within a model configuration that includes tidal forcing. It is shown, that assimilation of unfiltered (with tides) surface-current observations into the model with tides improves the sub-tidal model predictions to the level comparable with the assimilation of filtered data into the non-tidal model, which is significant with respect to options for designing real-time nowcast and forecast systems. Finally, the approach is extended and evaluated for the direct assimilation of HF radar-derived radial velocity components. The model runs that included assimilation of radials from at least two HF radar sites show better correlations with observations than the non-assimilative run, especially those runs that included radials from the Santa Cruz site. Directions of radials for that site coincide with the directions of dominant southward flow during upwelling events and the northward flow during relaxation events. Direct assimilation of radial currents extends the range of influence of the data into regions covered by only one HF radar site.

Published by Elsevier Ltd.

1. Introduction

During the last decade high-frequency (HF) radar systems have been installed operationally throughout the world. Assimilation of HF radar surface currents into oceanic models has been a subject of a number of studies (Lewis et al., 1998; Breivick and Sætra, 2001; Oke et al., 2002; Kurapov et al., 2003; Paduan and Shulman, 2004; Wilkin et al., 2005). Surface-current data assimilation experiments based on high-frequency radar observations in summer 1999 and 2000 were described in Paduan and Shulman (2004). In that study, low-pass-filtered surface currents were assimilated into a non-tidal circulation model of Monterey Bay based on a nested implementation of the Princeton Ocean Model (POM). That model was forced with either the 91-km-resolution winds from the Navy's Global Atmospheric Prediction System (NOGAPS; Rosmond et al., 2002) or 9-km resolution-winds from the Navy's Coupled Ocean/Atmosphere Mesoscale Prediction System (COAMPS^{TM}; Hodur et al., 2002). The evaluated assimilation scheme consists of two steps: the physical-space statistical analysis system (PSAS) is used to derive corrections to the model surface velocity based on comparisons with observed surface currents. Then corrections are projected downward through the frictional boundary layer assuming that the model-data velocity differences at the surface represent the top of a constant eddy viscosity Ekman boundary layer (see Paduan and Shulman, 2004, and Section 3 below). The underlying hypothesis in this procedure is that inadequate wind-stress forcing can be partially compensated by adjusting model currents toward the observed surface currents. It was shown that assimilation of CODAR-type HF radar data improved model simulations at mooring locations down to 120 m (which was well below the depths directly influenced by the Ekman-layer-assimilation procedure; Paduan and Shulman, 2004).

The present study represents a follow-on to the work of Paduan and Shulman (2004) that takes advantage of the data collected around Monterey Bay as part of the Autonomous Ocean

* Corresponding author.
E-mail address: igor.shulman@nrlssc.navy.mil (I. Shulman).

0967-0645/$ - see front matter Published by Elsevier Ltd.
doi:10.1016/j.dsr2.2008.08.004

Sampling Network Experiment (AOSN-II) in August–September 2003. Also important is the initiation of a high-resolution (3 km) COAMPS^{TM} atmospheric model nest covering the central California region that was first put in place during AOSN-II (Doyle et al., 2008). In this study, we address the following issues:

1. Impact of assimilation of low-pass-filtered HF radar surface currents on model predictions during AOSN-II time frame.
2. Impact of assimilation of unfiltered HF radar surface currents on model predictions during AOSN-II time frame. The data assimilation approach of Paduan and Shulman (2004) was designed for correcting wind-driven, sub-tidal currents. For this reason, the 33-h low-pass-filtered CODAR data were assimilated into the circulation model. Oke et al. (2002), for example, used a rather more computationally expensive pre-filtering in their data assimilation scheme to minimize shocks in the model responses. We investigate whether the assimilation of unfiltered data improves or degrades sub-tidal model predictions in comparison to the assimilation of pre-filtered observations.
3. Impact of assimilation of HF radar radials on model predictions during AOSN-II time frame. Benefits of direct radial velocity assimilation include the ability to avoid the total vector combination step and errors associated with geometric dilution of precision effects. The area of data influence can be extended by including some information in regions covered by just one HF radar site. Direct assimilation of radial velocity components also expands the possibility to assimilate HF radar data from ships and petroleum platforms. Formulation of the assimilation problem in terms of radial velocity components does, however, greatly expand the apparent number of observations that must be dealt with during each assimilation time step.

2. Observation and model descriptions

2.1. HF radar network

Surface-current observations used in this study were derived from a network of five SeaSonde-type HF radar instruments deployed in the region of Monterey Bay (Fig. 1). Those instruments, commonly referred to as CODAR-type HF radar systems, exploit information in the radiowave backscatter from the ocean surface to infer movement of the near surface water. Electromagnetic waves in the HF band (approximately 3–30 MHz) exhibit Bragg-resonant reflections from wind-driven gravity waves on the ocean surface whose physical wavelength is precisely 1/2 the wavelength of the transmitted radiowave. During the AOSN-II period in August–September 2003, four SeaSonde systems were operating at frequencies near 12.5 MHz and one system (in Moss Landing) was operating at 25.4 MHz, which meant that the Bragg-resonant scatter from the sea surface was due to gravity waves whose wavelengths were, approximately, 12 and 6 m, respectively.

Several studies have investigated the performance of the Monterey Bay HF radar network by comparing the radar-derived currents with in situ velocity observations and by comparing radar-to-radar velocity estimates on the over-water baselines between radar sites (e.g., Paduan and Rosenfeld, 1996; Paduan et al., 2006). Consistent uncertainty values emerge in the range of 10–15 cm/s for the remotely estimated velocities. In addition to those performance measures, Paduan and Shulman (2004) described monthly tabulations of cross shore and along shore velocity decorrelation scales based on earlier computations from the Monterey domain. These same uncertainty and decorrelation values are used in this study.

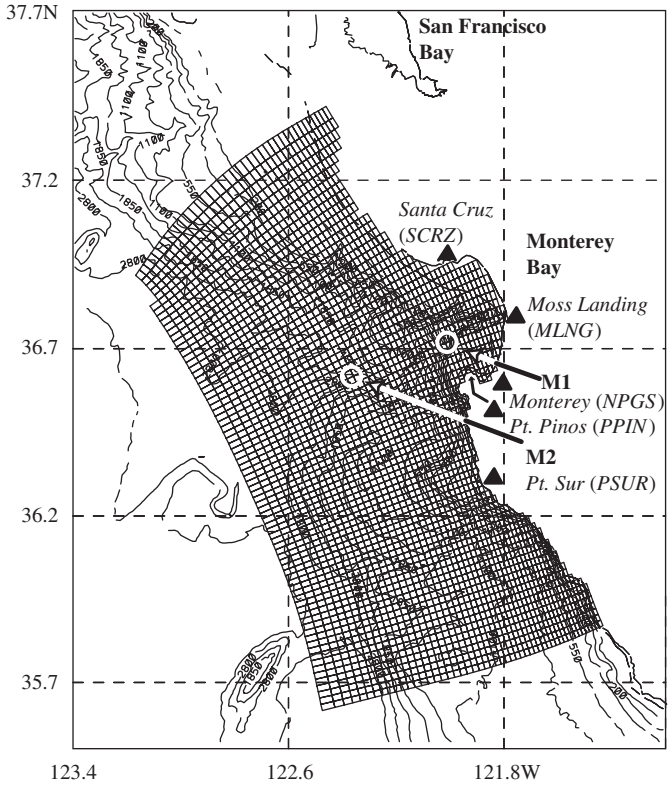

Fig. 1. The ICON model domain with local bathymetry and the locations of coastal HF radar sites (triangles) and offshore moorings (M1 and M2).

Also relevant to this study are the basic descriptions of data availability from the HF radar network. Each individual SeaSonde instrument provides a distribution of so-called "radial" velocity observations each hour on a polar coordinate grid centered on the radar site. Independent estimates of the speed of the water approaching or receding from the radar site are provided at scales of 3 km in range (1.5 km for the 25.4-MHz system) and 5° in azimuth. Each hour's spatial set of radial velocity estimates is not necessarily filled in. This is due to limitations of the direction finding algorithm used with a compact HF radar system such as the SeaSonde (see, for example, Barrick and Lipa, 1997; Laws et al., 2000; de Paolo and Terrill, 2007; Toh, 2005). The cumulative radial velocity coverages are shown in Fig. 2 for each radar site. In the figure, the value at each grid location depicts the percentage of the total possible hourly observations obtained at that location during the analysis period. From the figure, it can be seen that the offshore range for the 12.5-MHz systems was between about 50 and 60 km, while the range for the 25.4-MHz system was about 40 km. Vector current estimates require overlapping radial observations from two or more HF radar sites, which results in more limited coverage. Vector currents were estimated on a Cartesian grid with a horizontal resolution of 3 km by computing the best-fit vector velocity components using all radial velocity observations within a radius of 3 km for each grid point each hour (hence, neighboring vector current results are not completely independent). The percent coverages by grid location for (total) vector currents are also shown in Fig. 2.

Finally, it is important to point out what are the approximate depths of the HF radar-derived current estimates. Because the HF radar measurement depends on the ocean currents impeding or assisting the Bragg-resonant gravity waves, the depth or thickness of the relevant ocean currents depends on the penetration depths of the resonant wave's particle motions. The weighted averaged

Please cite this article as: Shulman, I., Paduan, J.D., Assimilation of HF radar-derived radials and total currents in the Monterey Bay area. Deep-Sea Research II (2008), doi:10.1016/j.dsr2.2008.08.004

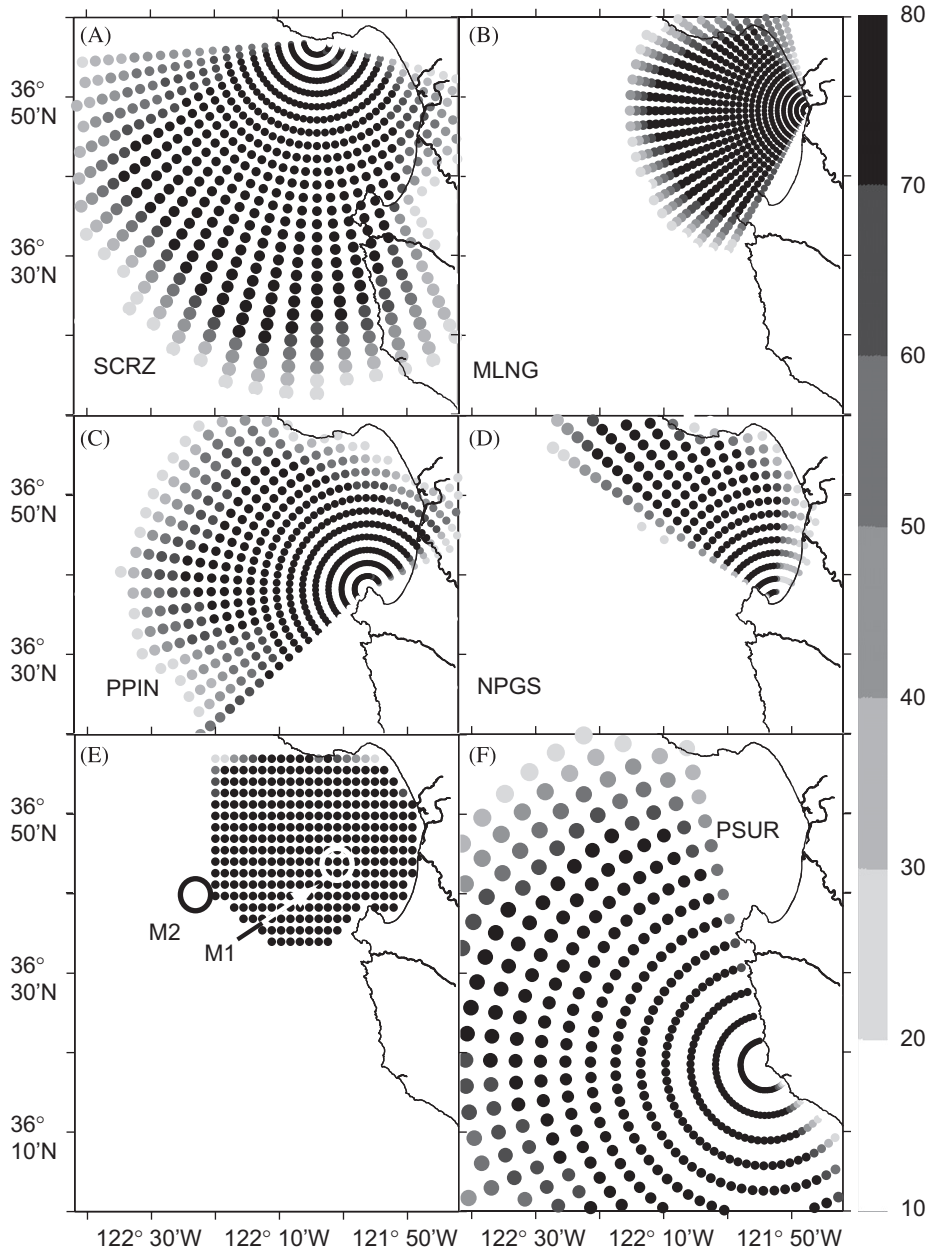

Fig. 2. Radial footprints and percent temporal coverage for HF radar sites: SCRZ (A; Santa Cruz), MLNG (B; Moss Landing), PPIN (C; Pt. Pinos), NPGS (D; Naval Postgraduate School), and PSUR (F; Pt. Sur). The footprint and temporal coverage for the vector analysis grid are shown along with the locations of moorings M1 and M2 (E).

depths of the measured currents are on the order of 0.8 and 0.5 m for HF radar measurements at 12.5 and 25.4-MHz, respectively (Stewart and Joy, 1974). Note: in this study we have ignored subtle differences expected for currents measured at these very near surface depths. In other cases, investigators have attempted to use simultaneous measurements over a range of frequencies to look for statistical differences in the measured velocities (e.g., Teague et al., 2001; Meadows, 2002).

2.2. Moored observations

For this study (August 6–September 6 of 2003), the model current predictions with and without assimilation of HF radar data were compared to currents measured by a 75-kHz RD Instruments Acoustic Doppler Current Profiler (ADCP) mounted in a downward-looking configuration on the Monterey Bay Aquarium Research Institute's (MBARI) surface moorings: at 122.02°W, 36.74°N, designated M1 and at 122.40°W, 36.67°N, designated M2 (see Fig. 1). For both moorings the ADCPs were set up to measure currents in 60 bins (8-m bins with the first bin at 16 m depth). Complex correlation and mean speed errors between the observed and model-predicted currents were used for comparisons. The magnitude ρ and the angular displacement θ of the complex correlation coefficient between the ADCP and the model currents for a particular depth were estimated using the approach outlined in Kundu (1976). The magnitude is estimated as:

$$\rho = \sqrt{\mathrm{Re}^2 + \mathrm{Im}^2}, \tag{1}$$

where

$$\mathrm{Re} = \frac{\sum_t (u_t^o u_t^m + v_t^o v_t^m)}{\sqrt{\sum_t ((u_t^o)^2 + (v_t^o)^2) \sum_t ((u_t^m)^2 + (v_t^m)^2)}},$$

Please cite this article as: Shulman, I., Paduan, J.D., Assimilation of HF radar-derived radials and total currents in the Monterey Bay area. Deep-Sea Research II (2008), doi:10.1016/j.dsr2.2008.08.004

$$\mathrm{Im} = \frac{\sum_t (u_t^o v_t^m + v_t^o u_t^m)}{\sqrt{\sum_t ((u_t^o)^2 + (v_t^o)^2) \sum_t ((u_t^m)^2 + (v_t^m)^2)}}.$$

The corresponding angular displacement θ, which is also called the phase angle, is computed according to:

$$\theta = \tan^{-1} \frac{\sum_t (u_t^o v_t^m - v_t^o u_t^m)}{\sum_t (u_t^o u_t^m + v_t^o v_t^m)} \quad (2)$$

where $u_t{}^m$, $v_t{}^m$ are the demeaned east–west and north–south model velocity components, respectively, and $u_t{}^o$, $v_t{}^o$ are the demeaned east–west and north–south observed velocity components, respectively. The angular displacement θ gives the average counterclockwise angle difference between model and observed velocity vectors.

In addition to the complex correlation, we compute a measure of error based on the average of the vector speed difference according to:

$$\mathrm{RMSE} \equiv \sum_t \frac{((U_t^o - U_t^m)^2 + (V_t^o - V_t^m)^2)^{1/2}}{N}, \quad (3)$$

where $U_t{}^m$, $V_t{}^m$ and $U_t{}^o$,$V_t{}^o$ are the total velocity components, i.e., not demeaned. N is the number of temporal samples.

2.3. The Monterey Bay model

The hydrodynamic model used in this study was described in detail in Shulman et al. (2002), Paduan and Shulman (2004), Ramp et al. (2005), and Rosenfeld et al. (2008). It is called the ICON model, which is a fine resolution ocean model covering Monterey Bay and the adjacent coastal areas (see model domain on Fig. 1). The horizontal resolution ranges from 1–4 km and there are 30 vertical sigma levels.

In this study, the ICON model was forced with 3-km resolution wind stresses and heat fluxes from the COAMPS predictions. Tidal forcing was introduced into the model through the specification of the open boundary conditions using tidal constants interpolated from the Oregon State University Tidal Solution (Egbert and Erofeeva, 2002) for the US West Coast. Eight tidal constituents (M2, S2, N2, K2, K1, O1, P1, Q1) were included.

On open boundaries the ICON model is coupled to the Pacific West Coast (PWC) model (Haidvogel et al., 2000; Rochford and Shulman, 2000) using the following Flather condition (Rochford and Shulman, 2000):

$$\overline{u_n} = \overline{u_n^o} + (g/H)^{1/2}(\eta - \eta^o) \quad (4)$$

with

$$\eta^o = \eta_{\mathrm{pwc}} + \eta_{\mathrm{tide}}$$
$$\overline{u_n^o} = \overline{u_{\mathrm{pwc}}} + \overline{u_{\mathrm{tide}}}, \quad (5)$$

where η is the model sea surface elevation on the open boundary, $\overline{u_n}$ is the model vertically averaged outward normal component of velocity on the open boundary, η_{pwc} and $\overline{u_{\mathrm{pwc}}}$ are a sea surface elevation and vertically averaged velocity from larger scale PWC model simulations (no tides). Respectively, η_{tide} and $\overline{u_{\mathrm{tide}}}$ are a tidal sea surface and vertically averaged tidal velocity predicted by using eight tidal constants from the OSU model (Egbert and Erofeeva, 2002). Details about the tides implementation, along with comparisons of vertical and horizontal patterns against those derived from moorings and HF radar are presented in Rosenfeld et al. (2008).

3. HF radar data assimilation approach

According to Paduan and Shulman (2004), the analysis (updated) field of the model surface currents is derived from (bold letters are vectors):

$$\mathbf{U}_\alpha^{\mathrm{a}} = \mathbf{U}_\alpha^{\mathrm{f}} + K(\mathbf{U}_\beta^o - H\mathbf{U}_\alpha^{\mathrm{f}}), \quad (6)$$

where $\mathbf{U}_\alpha{}^{\mathrm{a}}$ are the analyzed surface currents, $\mathbf{U}_\alpha{}^{\mathrm{f}}$ are the model forecast surface currents, $\mathbf{U}_\beta{}^{\mathrm{o}}$ are HF radar-derived surface currents, α indicates model grid locations, and β indicates observations locations. H is the interpolation operator of the model velocity from the model grid α to the observation locations β and the matrix K is the Kalman gain, which depends on the forecast error covariance matrix P^{f} and the observation error covariance matrix, R:

$$K = P^{\mathrm{f}} H^{\mathrm{T}} (H P^{\mathrm{f}} H^{\mathrm{T}} + R)^{-1}. \quad (7)$$

According to Eq. (6), corrections to the surface velocity $\delta\mathbf{U}_\alpha = \mathbf{U}_\alpha^{\mathrm{a}} - \mathbf{U}_\alpha^{\mathrm{f}} = (\delta u_\alpha, \delta v_\alpha)$ were applied to the surface layer of the model. These surface velocity corrections were assumed to be related to errors in the model wind forcing and were projected downward based on Ekman theory (for more details see Paduan and Shulman, 2004). P^{f} and R in Eq. (7) are described in Paduan and Shulman (2004), and estimated from observed HF radar covariance scales.

The above data assimilation approach is designed for correcting wind-driven, sub-tidal currents. All experiments in Paduan and Shulman (2004) were conducted using 33-h low-pass-filtered CODAR data assimilated into the circulation model without tidal forcing. With the implementation of tidal forcing into the Monterey Bay model, assimilation of unfiltered surface currents became more consistent with the model forcing functions. In the case of the model with tides, errors in tidal predictions will also contribute to the misfits between observed and model predicted surface currents (Rosenfeld et al., 2008). In this study, the same P^{f} and R were used for assimilation of filtered and unfiltered surface currents (the objective is to compare sub-tidal model predictions with assimilation of filtered and unfiltered data). The question here is whether the assimilation of unfiltered data improves or degrades sub-tidal model predictions. Being fully aware about possible drawbacks of the approach, answers to the above question are addressed in Section 4.1.

As was stated in the Introduction, another objective of the paper is development and testing of an approach for direct HF radar radial current assimilation. In that case, observations are projections of unknown observed vectors $\mathbf{U}_\beta^o = \{U_\beta^o, V_\beta^o\}$ on radial directions. The result is:

$$U_\beta^{o,\mathrm{p}} = (\mathbf{U}_\beta^o \mathbf{e}_{\mathrm{R}}) = U_\beta^o e_x^{\mathrm{R}} + V_\beta^o e_y^{\mathrm{R}} \quad (8)$$

where $\mathbf{e}_{\mathrm{R}}$ is a unit vector along the radial, and $U_\beta^{o,\mathrm{p}}$ is a projection of vector $\mathbf{U}_\beta{}^o$ on the radial direction. In (6) the operator H is just the interpolation operator of the model velocity to the locations of observations. In the case of radials assimilation, we introduce the operator H_{R}, which does the interpolation of the model velocity from the model grid α to the observations locations β and the projection of velocity onto the direction of the corresponding radial. Therefore, the operator H_{R} both interpolates model velocity and transforms vectors to scalars. The adjoint operator $\mathbf{H}_{\mathrm{R}}^{\mathrm{T}}$ transforms the scalar to a vector at the observational locations (hence the use of bold case for $\mathbf{H}_{\mathrm{R}}^{\mathrm{T}}$) and interpolates the vector back to the model grid locations:

$$(H_R \mathbf{U}_\alpha^{\mathrm{f}}, U_\beta^P) = (\mathbf{U}_\alpha^{\mathrm{f}}, \mathbf{H}_{\mathrm{R}}^{\mathrm{T}} U_\beta^P),$$

where

$$\mathbf{H}_{\mathrm{R}}^{\mathrm{T}} U_\beta^P = U_\beta^P \mathbf{e}_{\mathrm{R}}$$

In this case, instead of (6) we have:

$$\mathbf{U}_\alpha^{\mathrm{a}} = \mathbf{U}_\alpha^{\mathrm{f}} + \mathbf{K}_{\mathrm{R}}(U_\beta^{o,\mathrm{p}} - H_{\mathrm{R}} \mathbf{U}_\alpha^{\mathrm{f}}), \quad (9)$$

Please cite this article as: Shulman, I., Paduan, J.D., Assimilation of HF radar-derived radials and total currents in the Monterey Bay area. Deep-Sea Research II (2008), doi:10.1016/j.dsr2.2008.08.004

where, instead of (7), we have the following expression for Kalman gain $\mathbf{K}_R$:

$$\mathbf{K}_R = P^f \mathbf{H}_R^T (H_R P^f \mathbf{H}_R^T + R^P)^{-1}, \quad (10)$$

where R^P is the observational error covariance for radials. In practice, we solve first a linear system with unknown quantity q such that:

$$(H_R P^f \mathbf{H}_R^T + R^P) q = U_\beta^{o,p} - H_R \mathbf{U}_\alpha^f \quad (11)$$

and then the analyzed state $\mathbf{U}_\alpha{}^a$ is obtained from the equation:

$$\mathbf{U}_\alpha^a = \mathbf{U}_\alpha^f + P^f \mathbf{H}_R^T q. \quad (12)$$

4. Data assimilation experiments

To address the questions that we posed with regard to pre-filtering, wind resolution, and radial current assimilation, we conducted a series of model simulations. All analyses were conducted for the period 6 August–September 2003.

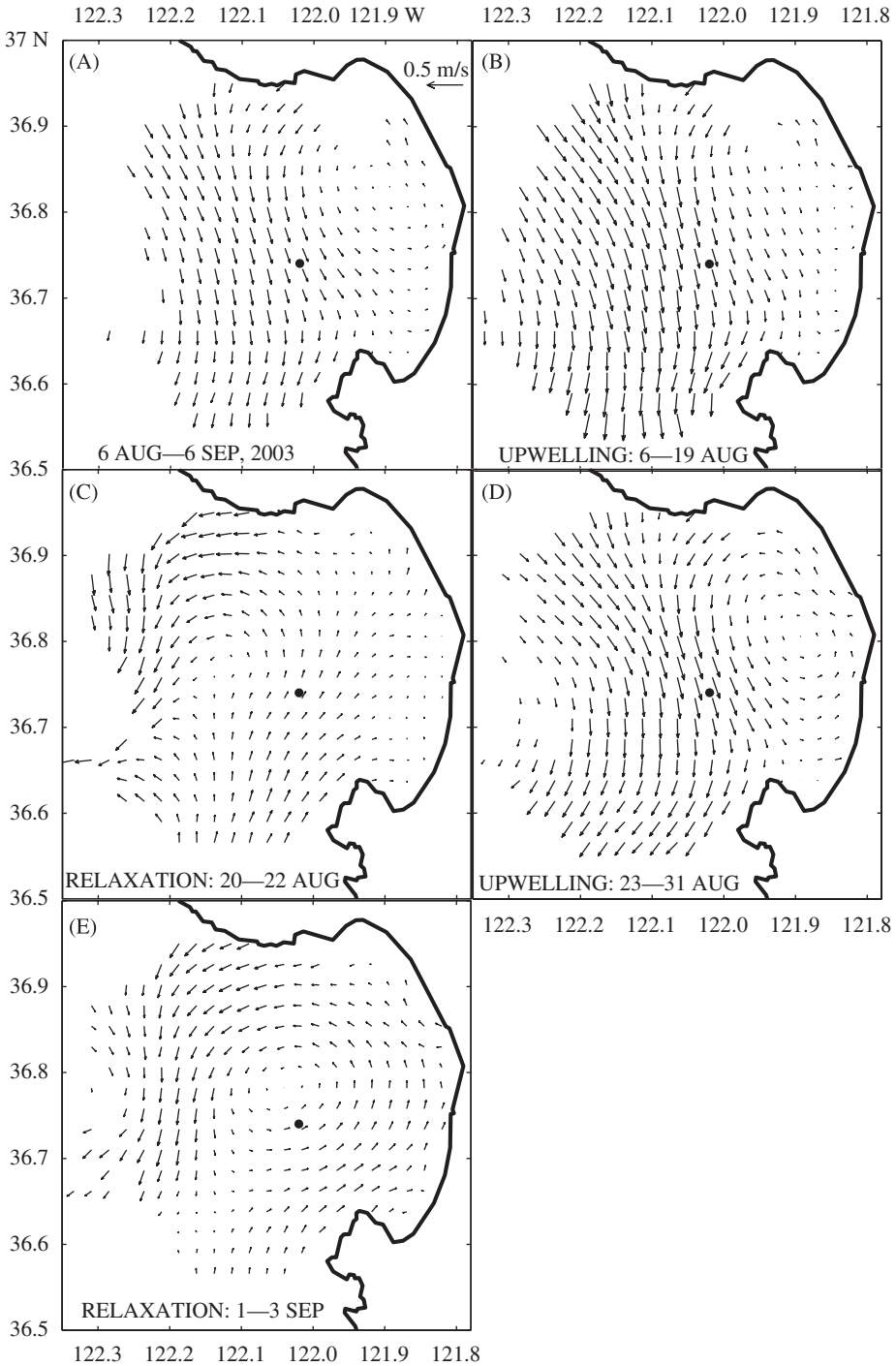

Fig. 3. CODAR surface currents averaged over: (A) entire time frame; (B) first upwelling (August 6–19); (C) first brief relaxation (August 20–22); (D) second extended upwelling (August 23–31) and (E) second brief relaxation (September 1–3). The symbol in each panel denotes the location of the M1 mooring (●).

Please cite this article as: Shulman, I., Paduan, J.D., Assimilation of HF radar-derived radials and total currents in the Monterey Bay area. Deep-Sea Research II (2008), doi:10.1016/j.dsr2.2008.08.004

As presented in Ramp et al. (2008), there were two extended upwelling events (August 6–19, and August 23–31), two very brief relaxation events (August 20–22, and September 1–3), and a weak upwelling (September 4–6) event. Fig. 3 shows CODAR surface currents averaged over the entire time frame and each of these identified events. During extended upwelling events, Fig. 3B and D indicate development of a strong southward-flowing jet along the entrance to the Bay. Note, that CODAR mean currents over the entire month are also southward near the M1 mooring (Fig. 3A). During the brief relaxation periods, when upwelling-favorable winds weaken, the structures are more complicated yet there is clear indication of the development of along-shore northward flow along the entrance to the Bay (Fig. 3C and E).

The distinct attributes of each model run are given in Table 1. All simulations were conducted using the same initial conditions and were forced with wind stress and heat fluxes from the 3-km-resolution COAMPS^{TM} atmospheric model analyses.

Table 1
Model and data configurations for various runs presented in this study

Run #	Surface current input data			Tidal forcing Included in model?
	Assimilation of low-pass-filtered?	Assimilation of unfiltered?	Sources[a]	
1	–	–	–	–
2	Yes	–	Vector	–
3	–	–	–	Yes
4	–	Yes	Vector	Yes
5	Yes	–	SCRZ, MLNG, PPIN, NPGS	–
6	Yes	–	SCRZ, MLNG	–
7	Yes	–	MLNG, PPIN	–
8	Yes	–	SCRZ, PPIN	–
9	Yes	–	SCRZ, PSUR	–
10	Yes	–	MLNG	–
11	Yes	–	SCRZ	–
12	Yes	–	PPIN	–
13	Yes	–	PSUR	–
14	Yes	–	SCRZ, MLNG, PPIN, NPGS, PSUR	–

4.1. Assimilation of HF radar surface currents

Run 1, which is without assimilation of surface-current data in the non-tidal model, is the control run for comparisons. Run 2 is a clone of Run 1 but filtered CODAR surface currents were assimilated. Run 3 is a clone of Run 1 but with tides included into the model forcing, and Run 4 is a clone of Run 3 but with assimilation of unfiltered CODAR surface currents into the model.

The 33-h low-pass-filtered observed and model-predicted currents at 48 m depth are shown in Fig. 4. A qualitative review shows that Runs 2 and 4 with assimilation of HF radar surface currents reproduced much better observed subsurface structure of currents at the M1 mooring.

Complex correlations and angular displacements between the model predicted and observed currents are shown at mooring locations M1 and M2 in Figs. 5 and 6, respectively.

Comparisons of complex correlations and angular displacements for Run 1 and Run 2 show that assimilation of filtered CODAR surface currents into the non-tidal circulation model significantly improves model current predictions. According to Fig. 5A, on average, the correlations with M1 currents increased from around 0.3–0.35 (Run 1) to around 0.7 (Run 2). Also, with

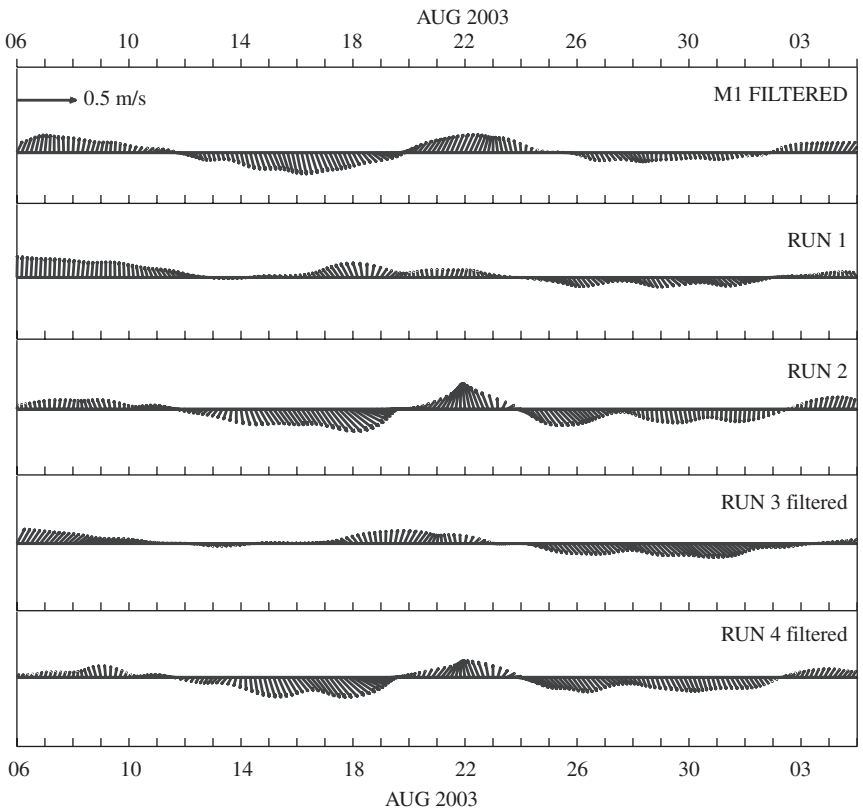

Fig. 4. 33-h low-pass-filtered observed and model-predicted currents at 48 m depth plotted every 4 h for the M1 mooring location.

Please cite this article as: Shulman, I., Paduan, J.D., Assimilation of HF radar-derived radials and total currents in the Monterey Bay area. Deep-Sea Research II (2008), doi:10.1016/j.dsr2.2008.08.004

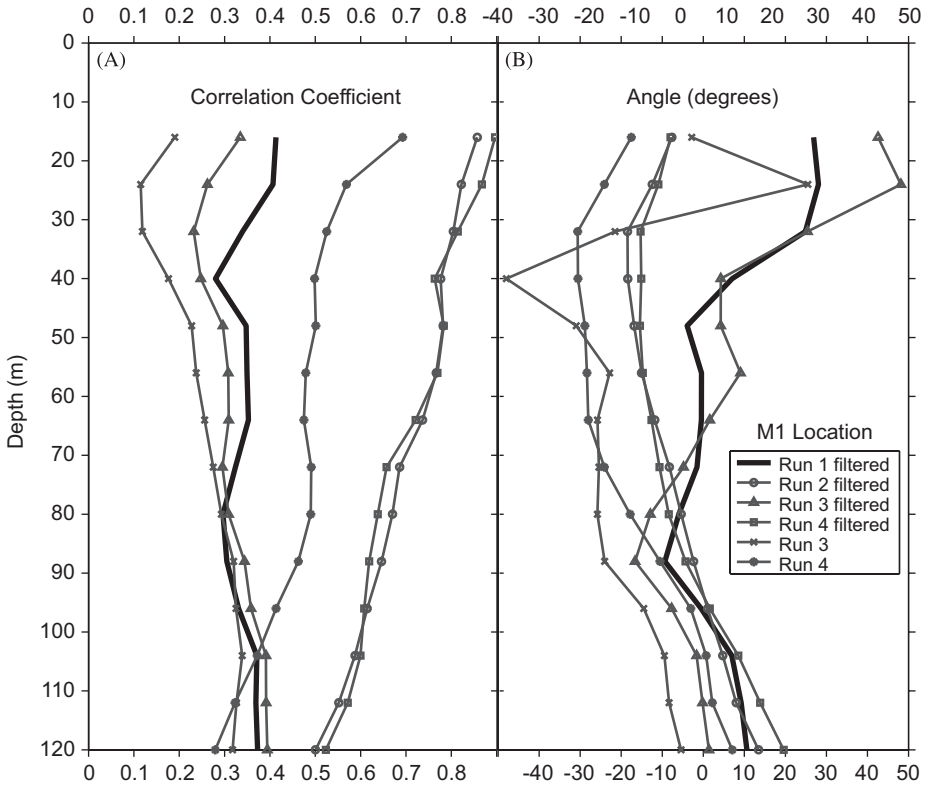

Fig. 5. Complex correlations (A) and angular displacements (B) between model-simulated and observed currents at mooring M1. The legend refers to model runs described in Table 1 and the notation "filtered" indicates that both model-simulated and observed currents were low pass filtered (33-h half-power point) prior to calculation of the complex correlations.

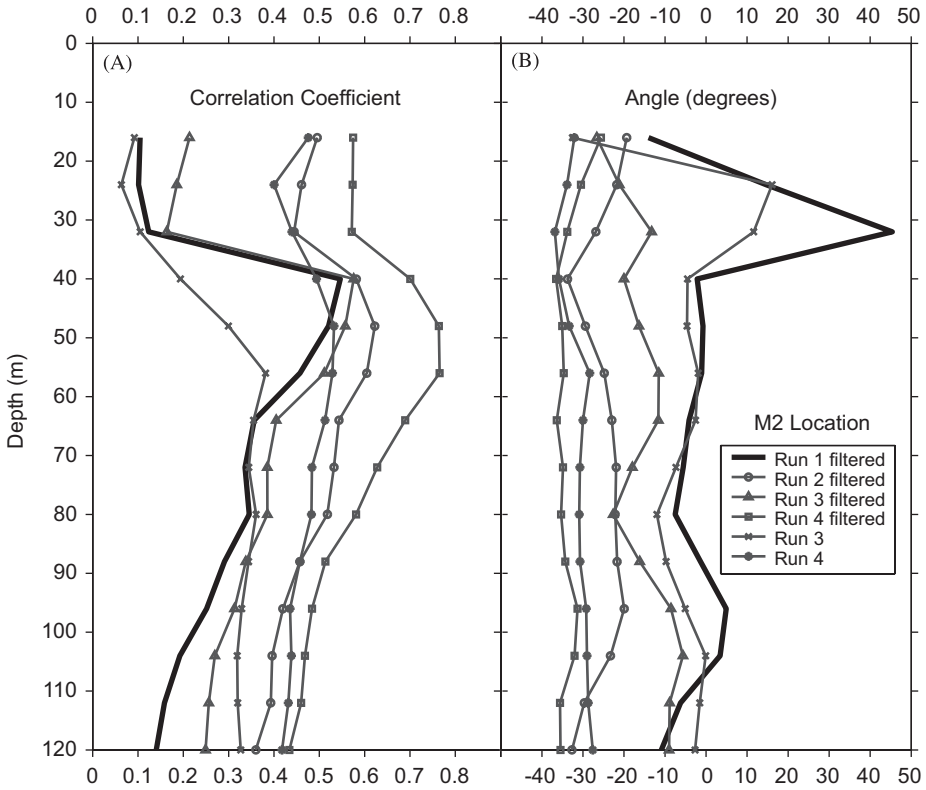

Fig. 6. As for Fig. 5 but at mooring M2.

Please cite this article as: Shulman, I., Paduan, J.D., Assimilation of HF radar-derived radials and total currents in the Monterey Bay area. Deep-Sea Research II (2008), doi:10.1016/j.dsr2.2008.08.004

assimilation the angle between model currents and observations (Fig. 5B) became smaller in the upper 40 m.

As we stated above, there were five upwelling/relaxation events during the considered time frame. With five degrees of freedom, a correlation value of 0.67 is significant with 95% confidence (see for example, Table XI of Hogg and Tanis (1993)). With this interpretation, correlations are significant down to 70 m depth for Runs 2 and 4 (filtered). However, we can suppose that the number of degrees of freedom is larger than five based on the shorter term fluctuations in the data set. There is strong diurnal variability in the atmospheric conditions in the area; correlations were estimated over a 31-day period using hourly data pass through a 33-h low-pass filter. This gives around 31*24/33∼22 samples. Therefore, the actual number of degrees of freedom is between 5 and 22. With 22 degrees of freedom a correlation of 0.34 is significant at the 95% confidence level. With that interpretation, correlations for Runs 2 and 4 (filtered) are significant for all depths shown on Fig. 5, and down to 100 m for Run 4 (unfiltered). Also, correlations for Run 1 are close to this significance level for many depths.

Note, that the value of angular displacement θ is only meaningful if complex correlation ρ is significant.

While correlations at M1 illustrate the impact of CODAR data assimilation on the model predictions inside the HF radar footprint (Fig. 1), the correlations at M2 illustrate the influence of assimilation on model predictions outside the footprint. Comparison of Runs 1 and 2 in Fig. 6 indicates an increase in correlation at M2 for the run with assimilation. This corresponds with results presented in Paduan and Shulman (2004), where it was demonstrated that assimilation of HF radar-derived surface currents improves model predictions not only in the area of the HF radar coverage but also outside of the area (for distant effect of data assimilation see also Kurapov et al., 2005).

On Figs. 5 and 6, curves labeled "Run 3 filtered" and "Run 4 filtered" show the impact of assimilation of unfiltered currents on sub-tidal predictions of the model with tides. There is a significant improvement in predictions of sub-tidal currents with the model assimilating unfiltered data. The model sub-tidal currents have similar correlation with observations in the case of assimilation of filtered data into the non-tidal model (Run 2) or with assimilation of unfiltered data into the model with tides (Run 4, filtered). Note that at mooring M2, correlation for "Run 4 filtered" is even better than for Run 2.

Correlation results are well supported by the RMSE values presented on Fig. 7 for the M1 and M2 locations. There is a decrease in RMSE in sub-tidal predictions due to assimilation of filtered as well as unfiltered surface-current data into the model without or with tides in comparison to the non-assimilative Run 1. This result is encouraging for real-time forecasting systems for which pre-filtering of observations is expensive and sometimes impossible.

The inclusion of tidal forcing in the circulation model appears to have introduced an additional source of error with respect to the mooring observations. This may not be surprising given that tidal currents in the region vary over small spatial scales (Rosenfeld et al., 2008). Location or phase errors in the modeled tidal currents can be expected to increase model-observation velocity differences. Results for unfiltered Runs 3 and 4 on Figs. 5–7 provides an estimate of the impact of surface current assimilation on total model current predictions. For example, there is a reduction in RMSE and a much better correlation for Run 4 with the surface current assimilation. According to Figs. 5 and 6, assimilation of surface-current data in Run 4 increased correlation at M1 from 0.2 (Run 3) to 0.7 at the surface and from around 0.3 to 0.5 on average in the subsurface; at M2 the correlation was increased to an average level of 0.45 in the upper 100 m.

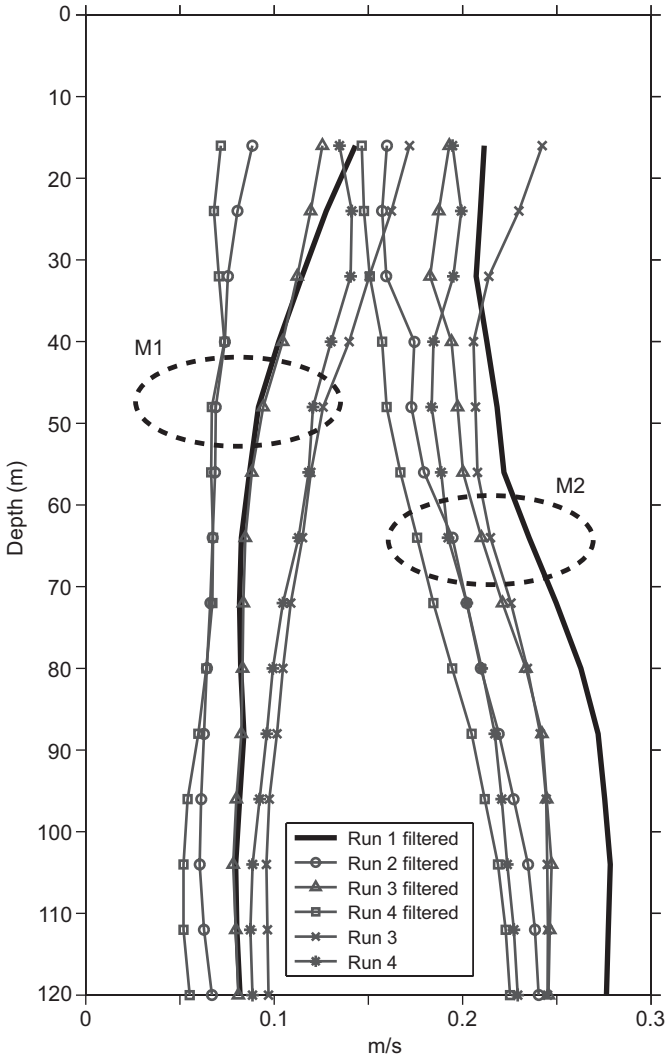

Fig. 7. RMSE, computed according to Eq. (3), between the model-simulated and observed currents at moorings M1 (left-hand group) and M2 (right-hand group). Dashed lines simply highlight the two sets of curves.

Surprisingly, the reductions in RMSE due to assimilation (Fig. 7) are larger at M2, which is just outside the surface-current coverage area, than they are at M1, which is in the center of the surface-current coverage (Fig. 2). We note also that RMSE for Run 3 with tides is significantly larger than that for the run without tides (Run 1).

To insure that the upper ocean results reflect the full impact of surface current assimilation, velocity difference statistics were investigated for a subset of the model runs using all available observation depths. Correlation magnitude and phase results for the control run (Run 1) versus the assimilation run (Run 2) are shown in Figs. 8 and 9 for the M1 and M2 locations, respectively. RMSE values for both mooring locations are shown in Fig. 10. Based on the correlation results, the positive effect of surface-current assimilation extends to about 140 m at M1 and to about 200 m at M2. Looking at the RMSE values in Fig. 10, it is clear that the absolute comparison between observed and simulated currents is better at M1 than at M2 for all depths. At mooring M1, the data assimilative run has smaller values of RMSE down to about 270 m depth, and slightly larger values below 270 m in comparison to the non-assimilative run. At mooring M2, the data assimilative run has smaller values of RMSE for all depths in comparison to the non-assimilative run. Overall, it appears that

Please cite this article as: Shulman, I., Paduan, J.D., Assimilation of HF radar-derived radials and total currents in the Monterey Bay area. Deep-Sea Research II (2008), doi:10.1016/j.dsr2.2008.08.004

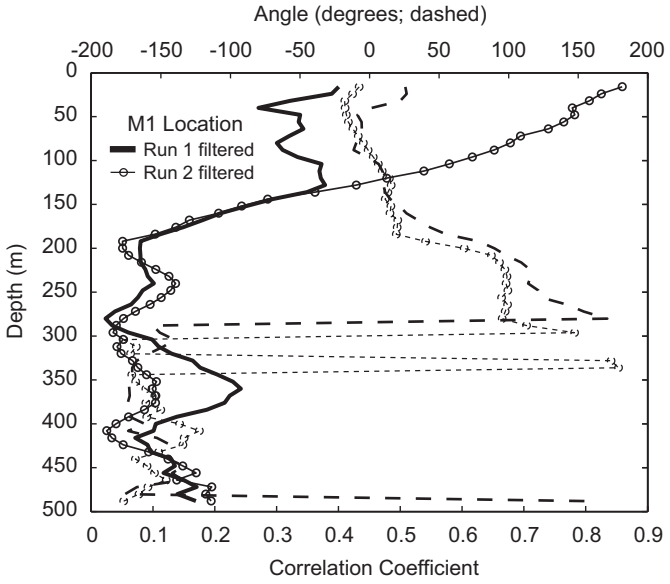

Fig. 8. Complex correlations (solid) and angular displacements (dashed) between model-simulated and observed currents at mooring M1 for Run 1 (bold) and Run 2 (thin). Both model-simulated and observed currents were low pass filtered (33-h half-power point) prior to calculation of the complex correlations.

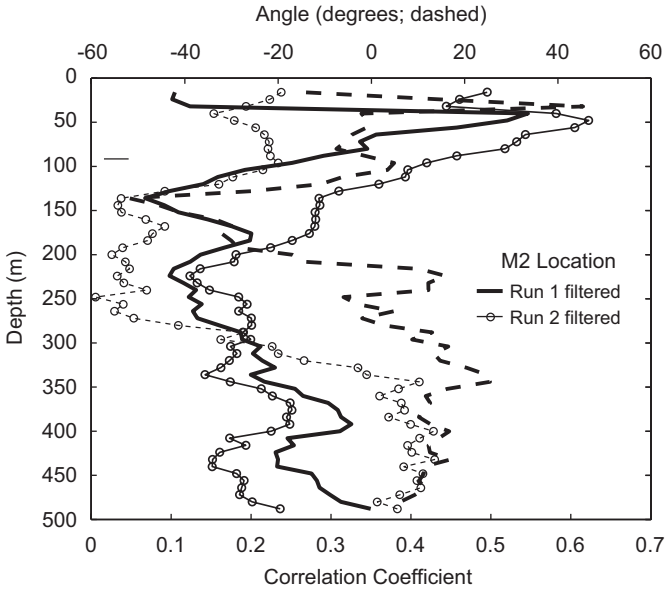

Fig. 9. As for Fig. 8 but at mooring M2.

the influence of surface-current assimilation is limited to the upper ocean within and above the main thermocline consistent with the correction-driven surface divergence mechanism proposed by Paduan and Shulman (2004), while the depth and magnitude of those influences can vary substantially for a given domain.

4.2. Assimilation of HF radar radials

Finally, we discuss results of the assimilation of radials from the five HF radar sites shown on Fig. 2. We note first that Run 2 and Run 4, which were discussed above, assimilated preprocessed vector surface currents based on input from four of the five sites: SCRZ, PPIN, MLNG, and NPGS. The resulting vector grid for those

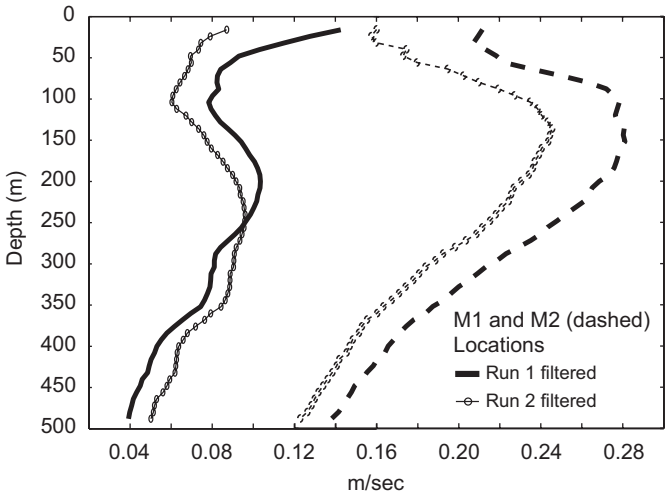

Fig. 10. RMSE, computed according to Eq. (3), between the model-simulated and observed currents at moorings M1 (left-hand group) and M2 (right-hand group) for Run1 (bold) and Run2 (thin). Both model-simulated and observed currents were low pass filtered (33-h half-power point) prior to calculation of the RMSE.

data is shown in Fig. 2E. Table 1 describes the attributes of all model runs, including Run 5 through Run 14 in which we assimilated radial surface current data from different combinations of the available HF radar sites. In these radial current runs, filtered observations of radials currents were assimilated into the model without tides.

Brief descriptions of physical conditions in the area were given in Section 4.1 and Figs. 3 and 4. For successful assimilation of radial current data, it is important to resolve the dominant along-shore component of the observed flow during upwelling/relaxation events, especially the southward flowing jet during extended upwelling events. Based on this, and the footprint of HF radar sites (Fig. 2), it is clear that sites MLNG, NPGS, and PSUR have limitations in resolving the flow around mooring M1. The MLNG radials are mostly oriented in the cross-shore direction and are, therefore, orthogonal to the direction of the dominant along-shore flow. Mooring M1 is located close to the boundaries of the data footprints for the NPGS and PSUR sites. Therefore, only the SCRZ and PPIN footprints cover the area around M1 well. While the direction of the SCRZ radials coincides nicely with the direction of dominant along-shore flow around the M1 mooring (Fig. 3), the PPIN site radials veer toward a cross-shore direction around M1 and, therefore, are expected to lose information about the major along-shore flow component. Also, the SCRZ footprint provides coverage of currents in extended areas upstream as well as downstream of M1, while the PPIN site provides limited coverage of the area to the south Pt. Pinos where northward flow develops during relaxation events.

Fig. 11 shows complex correlation magnitudes for various model runs (Table 1) based on comparisons with observed currents at M1. For reference, results for Run 1 (without assimilation) and Run 2 (with assimilation of preprocessed surface currents) are also included. Overall, complex correlation magnitudes for the runs with assimilation of radial surface currents are lower than those for Run 2 (with assimilation of preprocessed surface currents) at the M1 location. As it is stated in Section 2.1, HF radar vectors (before being assimilated in the Run 2) were estimated by computing the best-fit vector velocity components using all radial observations. In this case, around mooring M1, preprocessed HF radar surface currents represent better observed features than separate radials from multiple sites

Please cite this article as: Shulman, I., Paduan, J.D., Assimilation of HF radar-derived radials and total currents in the Monterey Bay area. Deep-Sea Research II (2008), doi:10.1016/j.dsr2.2008.08.004

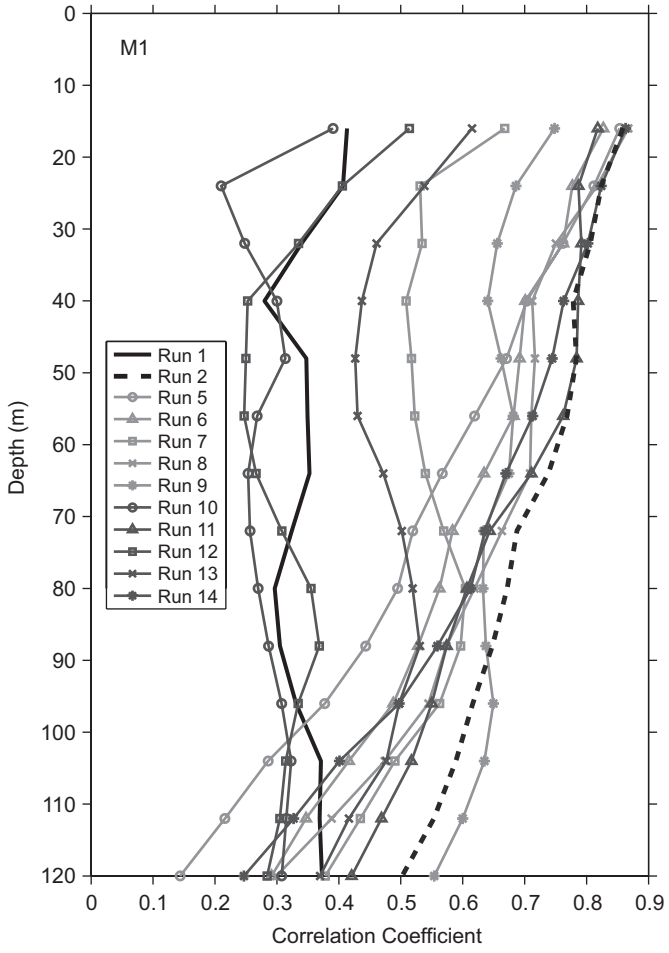

Fig. 11. Complex correlations between model-simulated and observed currents at mooring M1. The legend refers to model runs described in Table 1.

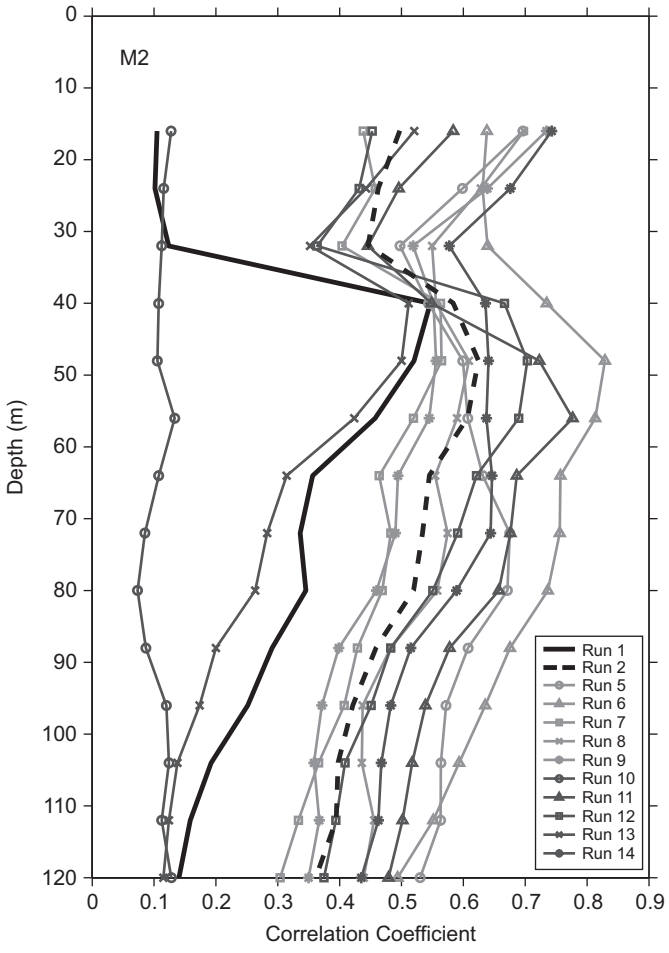

Fig. 12. As for Fig. 11 but at mooring M2.

(which are treated as independent observations in the data assimilation scheme of Section 3). At the same time, complex correlation magnitudes for the runs with assimilation of radials are higher than those for non-assimilative run (Run 1) at the M1 location. Only Run 10 (assimilation of only MLNG data) and Run 12 (assimilation of only PPIN data) have complex correlation magnitudes that are essentially the same as those for the non-assimilative run. As was hypothesized above, radials for the MLNG and PPIN sites do not resolve the dominant alongshore flow very well. Overall, model runs that included assimilation of radials from at least two HF radar sites show a better correlation than Run 1, especially those runs that included radial surface current data from the SCRZ site. This is in accord with the above hypothesis that the directions of radials for the SCRZ site coincide with the direction of dominant southward flow during upwelling events and the northward flow during relaxation events.

According to statistical significance discussions in Section 4.1, under an assumption of five degrees of freedom (five upwelling/relaxation events) correlations are significant down to 70 m depth for all runs with at least two sites assimilated (except Run 7 with MLNG and PPIN sites assimilated). Assuming 22 degrees of freedom (see explanations in Section 4.1) correlations for all runs (Fig. 11) are significant at least to 100 m depth, except for the non-assimilative run, and runs assimilating radials from the MLNG (Run 10) and PPIN (Run 12) sites.

Fig. 12 shows complex correlation magnitudes for various model runs based on comparisons with observed currents at M2. These results differ from those centered on the M1 mooring site. Assimilation of radials from only one site SCRZ (Run 11) show better correlations with observed currents at M2 than assimilation of preprocessed surface currents in Run 2 (Fig. 12). One of the reasons for this is that mooring M2 is located outside of the HF radar observational footprint for vector currents (Fig. 2E), while the footprint of the SCRZ site radials covers the M2 location (Fig. 2A). All Runs (Fig. 12) that include radial data from two sites, one of which is SCRZ, also perform better at the M2 location than Run 2 (for example, Runs 6 and 8).

Note, that the radial footprint of the PPIN site also reaches the M2 location. However, as shown above, the direction of radials for PPIN (Fig. 2C) do not resolve the dominant along-shore flow, which results in low correlations with observed currents at the M1 mooring. From Fig. 12, results from the assimilation of radials from only the PPIN site (Run 12) are worse in comparison to the assimilation of SCRZ radials (Run11), but are comparable to the results of Run 2.

The PSUR site radials also reach the M2 mooring. However, PSUR (Fig. 2F) has a coarser resolution footprint around the M2 mooring and the site is located far away in comparison to SCRZ and PPIN sites. As a result, correlations for Run 13, with assimilation of radials from only the PSUR site, are lower than those for runs with assimilation of radials from SCRZ and PPIN (Runs 11 and 12). However, the addition of radial data from PSUR in Run 14 (when data from all sites were assimilated) improved model predictions down to 70 m depth in comparison to Run 5 (using four other sites except PSUR). Overall, the assimilation of radial surface current data from four or five sites in Run 5 and Run

Please cite this article as: Shulman, I., Paduan, J.D., Assimilation of HF radar-derived radials and total currents in the Monterey Bay area. Deep-Sea Research II (2008), doi:10.1016/j.dsr2.2008.08.004

14, respectively, produced much better correlation with currents observed at M2 than did Run 2, which used vector current data whose observational footprint does not reach the M2 location.

The assimilation of radial surface-current data from just the MLNG site (Run 10) led to a dramatic decrease in the complex correlation magnitudes, especially for mid depths at M2, compared to Run 1 with no data assimilation. This is due to the fact that the MLNG radial footprint does not reach mooring M2, and, as it was stated above, radial directions do not resolve the dominant along-shore flow.

5. Conclusions

Paduan and Shulman (2004) conducted data assimilation experiments with input of 33-h low-pass-filtered surface current observations into the ICON circulation model without tides. The model wind forcing had either very coarse resolution (around 91 km) from the Navy's NOGAPS atmospheric circulation model or relatively fine resolution (around 9 km) from the Navy's COAMPS^{TM} model. In those cases, the assimilation improved model current predictions at the M1 and M2 mooring locations in Monterey Bay, and it was hypothesized that, at least, part of those results could be attributed to the HF radar-derived surface-current fields acting to correct for missing structure in the wind fields. In the present paper, the approach developed in Paduan and Shulman (2004) was applied to the assimilation of HF radar-derived surface-current data during the AOSN-II experiment time frame in August and September of 2003 when high-resolution (3 km) COAMPS^{TM} wind forcing was available. It was shown that assimilation of surface-current data has positive impacts on surface and subsurface model predictions even in cases for which high-resolution atmospheric forcing is used.

Another aspect of the present study involved an assessment of the role played by high-frequency velocity fluctuations. Currents in the Monterey Bay study area include significant contributions from internal tide fluctuations at the semi-diurnal period and sea breeze related fluctuations at the diurnal period (Rosenfeld et al., 2008). It has been an open question as to whether the inclusion of these velocity constituents within the data assimilation procedure would degrade the results achieved for sub-tidal period currents. The results presented here show that, under the present assimilation scheme, sub-tidal period velocity simulations are similarly improved through the assimilation of either low-pass-filtered surface currents or instantaneous (hourly) surface currents. This result is consistent with the mechanism proposed by Paduan and Shulman (2004) to explain the subsurface impacts of surface current assimilation. They suggested that model depths below the surface assimilation layer are influenced when the velocity correction field at the surface is horizontally divergent. The additional simulations described here also suggest that the subsurface impacts are driven by those divergences with time scales that are longer than the local inertial period, i.e. longer than the geostrophic adjustment time scale.

The option for direct assimilation of radial surface current observations from multiple HF radar sites also was demonstrated in the simulations described here. Overall, complex correlation magnitudes for the runs with assimilation of radial surface currents were lower than those for the run with assimilation of preprocessed surface currents at mooring M1, and higher at mooring M2. The model runs that included assimilation of radials from at least two HF radar sites show a better correlation than the non-assimilative run, especially those runs that included radials from the Santa Cruz site. Directions of radials for that site coincide with the direction of dominant southward flow during upwelling events and the northward flow during relaxation events. This result has practical implications in that single-component information from the radial current observations can be included from those portions of the model domain observed by just one HF radar site. In real-time applications, this approach will also allow processing to continue smoothly even when the available surface current coverage changes dramatically due to, for example, communication failures. At the same time, the impact of single-component radial data from individual HF radar sites was extremely variable. These facts point to the need to investigate further the impact of radial surface current assimilation, including the development of appropriate weighting schemes based on the independence and quality of individual radial current observations. Such figures of merit are being developed for other types of HF radar applications (e.g., Lipa, 2003; Kaplan and Lekien, 2007), which should be useful in future assimilation procedures.

In summary, we find this recently completed set of case studies to represent an encouraging step toward the practical use of remotely sensed surface-current mapping data in data assimilating coastal ocean models. Although the impact of surface-current data is limited to the upper ocean above, about, 120 m, improvement of model circulation fields in that depth range is important because it includes the euphotic zone and many of the most critical transport processes. The results are encouraging also because the coastal ocean area being mapped by HF radar instruments is growing rapidly making those instruments one of the essential components of the nation's integrated ocean-observing system.

Acknowledgments

This research was funded through the Naval Research Laboratory (NRL) under program element 61153N and by the Office of Naval Research under documents N00011405WX20794, N00011405WX20624, N0001403WX21141 and N0001403WX20819. We thank Leslie Rosenfeld of NPS for help with the tidal current implementation, and Jim Doyle of NRL Monterey for COAMPS^{TM} atmospheric forcing during the AOSN-II experiment. Our thanks also go to Mike Cook and Fred Bahr of NPS for providing assistance with the quality-control, processing, and presentation of the HF radar and mooring data, respectively. We thank Stephanie Anderson of NRL also for help with figures. Computer time for the numerical simulations was provided through a grant from the Department of Defense High Performance Computing Initiative. COAMPS^{TM} is a registered trademark of the Naval Research Laboratory. This manuscript is a NRL contribution 7330-06-7030.

References

Barrick, D.E., Lipa, B.J., 1997. Evolution of bearing determination in HF current mapping radars. Oceanography 10, 72–75.

Breivick, Ø., Sætra, Ø., 2001. Real-time assimilation of HF radar currents into a coastal ocean model. Journal of Marine Systems 28, 161–182.

de Paolo, T., Terrill, E., 2007. Skill assessment of resolving ocean surface current structure using compact-antenna-style HF radar and the MUSIC direction-finding algorithm. Journal of Atmospheric and Oceanic Technology 24, 1277–1300.

Doyle, J.D., Jiang, Q., Y. Chao, Ferrara, J., 2008. High-resolution real-time modeling of the marine atmospheric boundary layer in support of the AOSNII field compaign. Deep-Sea Research II, this issue [doi:10.1016/j.dsr2.2008.08.009].

Egbert, G.D., Erofeeva, S.Y., 2002. Efficient inverse modeling of barotropic ocean tides. Journal of Atmosphere and Oceanic Technology 19, 183–204.

Haidvogel, D.B., Blanton, J., Kindle, J.C., Lynch, D.R., 2000. Coastal ocean modeling: processes, and real-time systems. Oceanography 13 (1), 35–46.

Hodur, R.M., Pullen, J., Cummings, J., Hong, X., Doyle, J.D., Martin, P.J., Rennick, M.A., 2002. The coupled ocean/atmospheric mesoscale prediction system (COAMPS). Oceanography 15 (1), 88–98.

Hogg, R.V., Tanis, E.A., 1993. Probability and Statistical Inference. Prentice-Hall, Upper Saddle River, NJ, 731pp.

Kaplan, D.M., Lekien, F., 2007. Improved interpolation and extrapolation of surface current data based on modal current decomposition. Journal of Geophysical Research 112, C12007.

Kundu, P.K., 1976. Ekman veering observed near the ocean bottom. Journal of Physical Oceanography 6, 238–242.

Kurapov, A.L., Egbert, G.D., Allen, J.S., Miller, R.N., Erofeeva, S.Y., Kosro, P.M., 2003. The M_2 internal tide off Oregon: inferences from data assimilation. Journal of Physical Oceanography 33, 1733–1757.

Kurapov, A.L., Allen, J.S., Egbert, G.D., Miller, R.N., Kosro, P.M., Levine, M., Boyd, T., 2005. Distant effect of assimilation of moored ADP currents into a model of coastal wind-driven circulation off Oregon. Journal of Geophysical Research 110, C02022.

Laws, K., Fernandez, D.M., Paduan, J.D., 2000. Simulation-based evaluations of HF radar ocean current algorithms. Journal of Oceanic Engineering 25, 481–491.

Lewis, J.K., Shulman, I., Blumberg, A.F., 1998. Assimilation of CODAR observations into ocean models. Continental Shelf Research 18, 541–559.

Lipa, B.J., 2003. Uncertainties in SeaSonde current velocities. In: Proceedings of the IEE/OES Seventh Working Conference on Current Measurement Technology, San Diego, CA, pp. 95–100.

Meadows, L.A., 2002. High frequency radar measurements of friction velocity in the marine boundary layer. Ph.D. Dissertation, University of Michigan, Ann Arbor, 139pp.

Oke, P.R., Allen, J.S., Miller, R.N., Egbert, G.D., Kosro, P.M., 2002. Assimilation of surface velocity data into a primitive equation coastal ocean model. Journal of Geophysical Research 107 (C9), 3122.

Paduan, J.D., Rosenfeld, L.K., 1996. Remotely sensed surface currents in Monterey Bay from shore-based HF radar (CODAR). Journal of Geophysical Research 101, 20669–20686.

Paduan, J.D., Shulman, I., 2004. HF radar data assimilation in the Monterey Bay area. Journal of Geophysical Research 109, C07S09.

Paduan, J.D., Kim, K.C., Cook, M.S., Chavez, F.P., 2006. Calibration and validation of direction-finding high frequency radar ocean surface current observations. IEEE Journal of Oceanic Engineering, 862–875.

Ramp, S.R., Paduan, J.D., Shulman, I., Kindle, J., Bahr, F.L., Chavez, F., 2005. Observations of upwelling and relaxation events in the northern Monterey Bay during August 2000. Journal of Geophysical Research 110, C07013.

Ramp, S.R., Davis, R.E., Leonard, N.E, Shulman, I., Chao, Y., Robinson, A.R., Marsden, J., Lermusiaux, P., Fratantoni, D., Paduan, J.D., Chavez, F., Bahr, L., Liang, S., Leslie, W., Li, Z., 2008. Preparing to predict: the second autonomous ocean sampling network (AOSN-II) experiment in the Monterey Bay. Deep-Sea Research II, this issue [doi:10.1016/j.dsr2.2008.08.013].

Rochford, P.A., Shulman, I., 2000. Boundary conditions in the pacific west coast Princeton Ocean Model of CoBALT. NRL Technical Report, NRL/MR/7330-00-8245, 18pp

Rosenfeld, L.K., Shulman, I., Cook, M.S., Paduan, J.D., Shulman, L., 2008. Methodology for a regional tidal model evaluation, with application to central California. Deep-Sea Research II, this issue [doi:10.1016/j.dsr2.2008.08.007].

Rosmond, T.E., Teixeira, J., Peng, M., Hogan, T.F., Pauley, R., 2002. Navy Operational Global Atmospheric Prediction System (NOGAPS): forcing for ocean models. Oceanography 15, 99–108.

Shulman, I., Wu, C.R., Lewis, J.K., Paduan, J.D., Rosenfeld, L.K., Kindle, J.C., Ramp, S.R., Collins, C.A., 2002. High resolution modeling and data assimilation in the Monterey Bay area. Continental Shelf Research 22, 1129–1151.

Stewart, R.H., Joy, J.W., 1974. HF radar measurement of surface current. Deep-Sea Research 21, 1039–1049.

Teague, C.C., Vesecky, J.F., Hallock, Z.R., 2001. A comparison of multifrequency HF radar and ADCP measurements of near-surface currents during COPE-3. IEEE Journal of Oceanic Engineering 26, 399–405.

Toh, K.Y.D., 2005. Evaluation of surface current mapping performance by SeaSonde high frequency radar through simulations. M.S. Thesis, Naval Postgraduate School, Monterey, California, 123pp.

Wilkin, J.L., Arango, A.G., Haidvogel, D.B., Lichtenwalner, C.S., Glenn, S.M., Hedström, K.S., 2005. A regional ocean modeling system for the long-term ecosystem observatory. Journal of Geophysical Research 110, C06S91.

Please cite this article as: Shulman, I., Paduan, J.D., Assimilation of HF radar-derived radials and total currents in the Monterey Bay area. Deep-Sea Research II (2008), doi:10.1016/j.dsr2.2008.08.004